AIAA JOURNAL
Vol. 32, No. 4, April 1994

Two-Dimensional Unsteady Leading-Edge Separation on a Pitching Airfoil

P. Ghosh Choudhuri* and D. D. Knight†
Rutgers University, Piscataway, New Jersey 08855
and
M. R. Visbal‡
U.S. Air Force Wright Laboratory, Wright-Patterson Air Force Base, Ohio 45433

The initial stages of two-dimensional unsteady leading-edge boundary-layer separation of laminar subsonic flow over a pitching NACA-0012 airfoil have been studied numerically at Reynolds number (based on airfoil chord length) $Re_c = 10^4$, Mach number $M_\infty = 0.2$, and nondimensional pitch rate $\Omega_0^+ = 0.2$. Computations have been performed using two separate algorithms for the compressible laminar Navier-Stokes equations. The first method, denoted the structured grid algorithm, utilizes a structured, boundary-fitted C grid and employs the implicit approximate-factorization algorithm of Beam and Warming. The second method, denoted the unstructured grid algorithm, utilizes an unstructured grid of triangles and employs the flux-difference splitting method of Roe and a discrete representation of Gauss' theorem for the inviscid and viscous terms, respectively. Both algorithms are second-order accurate in space and time and have been extensively validated through comparison with analytical and previous numerical results for a variety of problems. The results show the emergence of a primary clockwise-rotating recirculating region near the leading edge which can be traced to a pair of critical points (a center and a saddle) that appear within the flowfield, followed by a secondary counterclockwise-rotating recirculating region and a tertiary clockwise-rotating recirculating region. The primary and secondary recirculating regions interact with each other to give rise to the unsteady separation ("breakaway") of the boundary layer.

I. Introduction

THE aerodynamics of unsteady airfoil motion is crucial to the performance of rotorcraft. The motion of a typical rotorcraft airfoil is complex. The main rotor of a conventional helicopter executes a complicated three-dimensional motion involving flapping (pitching), coning, and lagging.[1] To achieve a better understanding of the fluid motion, it is reasonable (and common) to separately study the individual elements of the airfoil motion (e.g., pitching) but recognize that the fluid physics is not so readily separable.

The understanding of boundary-layer separation is the key to understanding the viscous effects in unsteady aerodynamics. Qualitatively, boundary-layer separation is the breakdown of the boundary-layer model which divides the flow into two weakly interacting regions (i.e., an irrotational flow occupying most of the fluid volume and a thin viscous region adjacent to the solid boundary). For two-dimensional steady flows, the criterion for boundary-layer separation is well known and is indicated by the appearance of zero shear stress at the surface. For two-dimensional unsteady flows, however, the vanishing surface shear stress does not guarantee separation.[2] Rather, the appearance of a zero shear stress and zero velocity point within the fluid in a frame of reference traveling with the separation region seems to be the accepted criterion[3] (the "Moore-Rott-Sears" condition).

Boundary-layer separation is an integral part of the dynamic stall process which is characterized by a sudden decrease in lift and an equally dramatic change in pitching moment. The breakdown of the boundary layer (separation) leads to the formation of the dynamic stall vortex—a large recirculating region above the airfoil. (A recirculating region can be defined as a flow possessing vorticity with closed streamlines.) The subsequent motion of the dynamic stall vortex is a principal contributor to the variation in the airfoil lift and moment. Thus, the study of separation on a pitching airfoil is essential to development of a complete understanding of the dynamic stall process.

The general focus of the present research is subsonic viscous flow past a pitching airfoil. Extensive reviews of experimental and theoretical (analytical and numerical) research have been presented by Carr[4] and Carr and McCroskey.[5] Experimental studies have initiated modern research in unsteady flow past pitching airfoils and continue to provide critical information and insight. McCroskey et al.[6] described three different types of boundary-layer separation using oil smoke visualization. Acharya and Metwally[7] categorized and quantified the sources of vorticity. Chandrashekhara and Ahmed[8] measured the instantaneous velocity field. Carr et al.[9] studied dynamic stall using real time interferometry. Chandrashekhara and Carr[10] visualized the effects of Mach number on the dynamic stall of an oscillating airfoil. Computational studies have become increasingly useful in developing an understanding of the unsteady flow behavior. Mehta[11,12] calculated laminar flow past a pitching airfoil at Reynolds numbers (based on the airfoil chord) $Re_c = 5 \times 10^3$ and 10^4. Ghia et al.[13,14] successfully compared their computational results with the previous computations of Mehta[12] and the experimental results of Walker et al.[15] for $Re_c = 10^4$ and $Re_c = 4.5 \times 10^4$ and also studied some control strategies to delay the dynamic stall. Visbal[16] described the dynamic stall process for a pitching NACA-0015 airfoil as a highly complex, high Reynolds number flow phenomenon and presented some investigations of various flow control techniques. He also investigated the effects of compressibility on the dynamic stall and found that the ap-

Received Feb. 5, 1993; revision received Sept. 13, 1993; accepted for publication Sept. 27, 1993.

*Graduate Research Assistant, Department of Mechanical and Aerospace Engineering.
†Professor, Department of Mechanical and Aerospace Engineering. Associate Fellow AIAA.
‡Aerospace Engineer. Member AIAA.

pearance of the shock at high Mach numbers leads to an additional mechanism of dynamic stall process due to the shock/boundary-layer interaction.[17] Recent analytical studies have added to the fundamental understanding of unsteady separation and provided physical insight. Smith[18–20] examined several important issues including the instability of the leading-edge separation bubble and finite time breakup of the boundary layer. Peridier et al.[21,22] examined the interaction of a vortex with a boundary layer. Some additional research has also focussed on some geometrically simpler configurations such as a circular cylinder set into motion impulsively.[23,24] These studies have led to a better understanding of the spatial/temporal scales and phenomena associated with the breakdown of the boundary layer and onset of dynamic stall.[25,26]

The principal objective of the present paper is the understanding of the initial stages (incipient separation) of the unsteady subsonic leading-edge boundary-layer separation process for a NACA-0012 airfoil. Figure 1 shows schematically the various stages of the boundary-layer separation over a pitching airfoil, where instantaneous streamlines are displayed in a frame of reference attached to the airfoil. This paper deals with the understanding of the stages preceding dynamic stall, i.e., from zero angle of attack (a) up to (but not including) dynamic stall (e).

The flow conditions selected are $Re_c = 10^4$, $M_\infty = 0.2$, and nondimensional pitch rate $\Omega_0^+ = 0.2$, where $\Omega^+ = \Omega c/U_\infty$ (where Ω is the pitch rate in rad/s, c is the chord length, and U_∞ is the freestream velocity). The airfoil is pitched about the quarter chord axis. Computations have been performed using two different numerical algorithms. The first algorithm, denoted the structured grid algorithm, is an approximate-factorization implementation of Beam-Warming's method[27] using a structured, boundary-fitted grid system. The second algorithm,[28] denoted the unstructured grid algorithm, employs an unstructured grid of triangles and utilizes the flux-difference splitting method of Roe[29] for the inviscid fluxes and a discrete representation of Gauss' theorem for the viscous fluxes and heat transfer. The structured grid algorithm is implicit, whereas the unstructured grid algorithm is explicit. Both algorithms are second-order accurate in space and time. The use of different numerical algorithms provides a stringent examination of the accuracy of the computations.

The flow conditions were selected on the basis of simplicity and feasibility. The Reynolds number was chosen to insure laminar flow, thereby eliminating the inherent uncertainties associated with engineering turbulence models. To be sure, the present Reynolds number is significantly less than typical flight Reynolds numbers for rotorcraft applications. Nonetheless, the selected Reynolds number may be sufficiently large to provide qualitative insight into the practical case, as the boundary-layer separation near the leading edge can be laminar in practice[30] with transition to turbulence following. The Mach number M_∞ was selected to insure subsonic flow at the chosen Re_c and Ω_0^+. The local Mach number does not exceed 0.6 throughout the entire pitching motion.

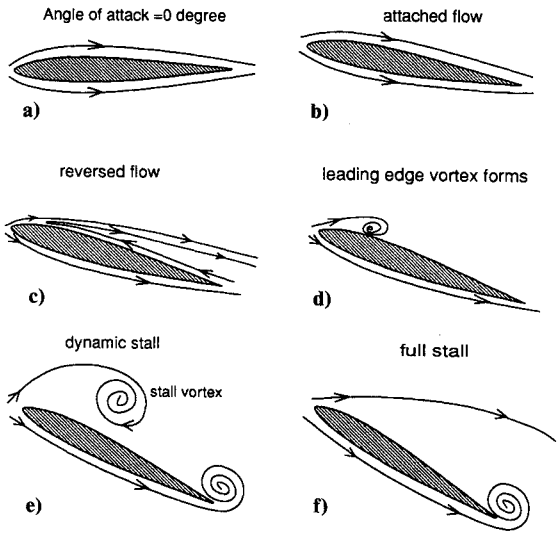

Fig. 1 Stages in pitching motion of an airfoil.

II. Details of Computation

A. Governing Equations

The governing equations are the two-dimensional unsteady compressible laminar Navier-Stokes equations written in strong conservation form.[31] The equations are written in an inertial frame of reference. The flow variables are nondimensionalized using the dimensional reference quantities chord length c, freestream density ρ_∞, freestream velocity U_∞, and static temperature T_∞. The dynamic molecular viscosity is assumed to satisfy Sutherland's relation.[32] The perfect gas law and a constant Prandtl number ($Pr = 0.73$ for air) provide closure of the system of equations.

B. Structured Grid

1. Numerical Algorithm

The implicit approximate-factorization method of Beam and Warming[27] employs a structured, boundary-fitted grid. The algorithm is implemented in the delta form with trapezoidal temporal differencing and central spatial differencing, which have second-order temporal and spatial accuracies. Fourth-order explicit and second-order implicit numerical damping is employed to eliminate spurious numerical oscillations.[33] The motion of the airfoil is included through a general time dependent coordinate transformation $\{\xi = \xi(x, y, t), \eta = \eta(x, y, t), \tau = t\}$.

Suitable boundary conditions are specified along the boundaries of the computational domain. At the airfoil surface, the no-slip condition is applied to the velocity. The normal temperature gradient is zero (adiabatic wall). The normal pressure gradient is obtained from the momentum equation and incorporates the effect of the airfoil motion.[17,34] A C-grid topology (Fig. 2) is employed, and the periodicity condition at the branch cut is imposed implicitly. At the entire outer boundary of the computational domain, a one-dimensional unsteady method of characteristics boundary condition[35] is employed. The effect of the outer boundary distance on the computed results has been studied and the outer boundary defined at a sufficiently large distance from the airfoil to insure accuracy of this boundary condition.

The implicit, unsteady, two-dimensional compressible, laminar Navier-Stokes solver was developed originally by Visbal[34,36,37] for an O-grid topology. Principal modifications

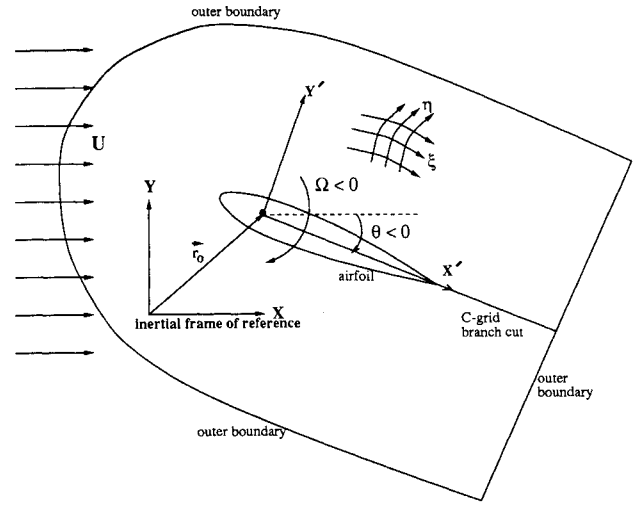

Fig. 2 Pitching airfoil and C-grid topology.

include the incorporation of a C-grid, the method of characteristics boundary condition at the outer boundary and the geometric conservation law[38] to eliminate the grid movement related errors in the governing equations.

The nearly orthogonal boundary-fitted C grid was generated by the hyperbolic grid generation code developed by Kinsey and Barth.[39]

2. Validation of Algorithm

A series of test computations were performed to establish the accuracy of the structured grid algorithm.

a) Flat plate boundary layer. The freestream Mach number M_∞ was 2.0, and Reynolds number Re_L (based on the plate length L) was 10^4. A linear viscosity law $\mu/\mu_\infty = T/T_\infty$ was employed with $Pr = 1$. The grid employed $N_\xi = 60$ and $N_\eta = 75$ grid points in the streamwise (ξ) and normal (η) directions, respectively. The number of grid points within the boundary layer was $N_{BL} = 54$ at $x = L$.

The computed velocity and static temperature profiles agreed with the analytical[32] profiles within 0.7% and 0.9%, respectively.

b) Stationary airfoil (NACA-0012). The freestream Mach number was $M_\infty = 0.2$, angle of attack was $\alpha = 0$ deg, Reynolds number was $Re_c = 5 \times 10^3$, and the nondimensional pitch rate was $\Omega_0^+ = 0$. A C grid was employed with $N_\xi = 303$ and $N_\eta = 101$ where ξ is the curvilinear coordinate in the direction of the C, and η is the coordinate approximately orthogonal to ξ. The average normal distance of the first row of mesh points adjacent to the airfoil was $\Delta n_{aver} = 5.0 \times 10^{-4}c$, and 25 grid points were contained within the boundary layer at midchord. The grid spacing tangential to the airfoil surface varied from $\Delta s = 4.3 \times 10^{-4}c$ to $1.99 \times 10^{-2}c$, with the finest grid employed near the leading and trailing edges.

The computed drag coefficient of the present study shows close agreement with the previous computation of Beran[40] at the same flowfield conditions, and similar agreement with the previous computation of Mehta[12] at the same Reynolds number for incompressible flow (Table 1). Detailed comparison with the surface pressure coefficient showed similar close agreement.

The computed flowfield was found to be insensitive to the magnitude of the explicit damping coefficient ω_e provided $\omega_e < 0.01$. The computed drag coefficient was $c_d = 0.05431$ and 0.05435 for $\omega_e = 0.005$ and 0.010, respectively. Also, the computed flowfield was observed to be insensitive to the location of the outer boundary provided the distance from the airfoil exceeded $18c$. For example, the computed drag coefficient was found to be $c_d = 0.05439$ and 0.05443 for outer boundary locations of $18c$ and $30c$, respectively.

c) Pitching airfoil (NACA-0015). The freestream Mach number was $M_\infty = 0.2$, the Reynolds number was $Re_c = 10^4$, and the nondimensional pitch rate was $\Omega_0^+ = 0.2$. The pitching motion was defined by

$$\Omega(t) = \Omega_0\{1 - \exp(-4.6t/t_0)\} \quad (1)$$

where Ω is the pitch rate in rad/s, t_0 is the time at which Ω has reached 99% of the asymptotic value Ω_0, and $\Omega_0 c/U_\infty = \Omega_0^+ = 0.2$. The flow conditions and expression for $\Omega(t)$ correspond to the previous computation by Visbal.[37] The airfoil was pitched about the quarter chord axis. The functional form of $\Omega(t)$ provides a smooth acceleration of the airfoil to its asymptotic pitching rate Ω_0 during an effective time interval $t_0 = 0.5c/U_\infty$ which corresponds to 4.57 deg of pitch.

Table 1 Computed drag coefficient (stationary NACA-0012 airfoil) $Re_c = 5 \times 10^3$, $M_\infty = 0.2$, $\alpha = 0$ deg

Reference	Drag coefficient c_d
Structured grid	0.0544
Unstructured grid	0.0547
Beran	0.0530
Mehta	0.0534

A C grid was employed with $N_\xi = 332$ and $N_\eta = 85$. The average normal distance of the first row of mesh points adjacent to the airfoil was $\Delta n_{aver} = 1.0 \times 10^{-4}c$, and 33 grid points were contained within the boundary layer at midchord. The grid spacing tangential to the airfoil surface varied from $\Delta s = 4.59 \times 10^{-3}c$ to $1.47 \times 10^{-2}c$, with the finest grid employed near the leading and trailing edges.

The computed flowfields were found to be in close agreement with the previous computation by Visbal.[37] In particular, the computed lift coefficient c_l and drag coefficient c_d agreed with the previous results of Visbal to within 4.0% for $0 < \alpha < 25$ deg, where α is the angle of attack of the airfoil. Detailed examination of the flow variables showed similar close agreement.

C. Unstructured Grid

1. Numerical Algorithm

The algorithm employs an unstructured grid of triangles which form the control volumes for application of the governing equations. The inviscid fluxes are obtained from the flux difference split method of Roe[29] using second-order accurate linear reconstruction of the conservative variables to the cell faces.[41] The viscous fluxes and heat transfer are obtained from application of Gauss' theorem.[42] The values of the conservative variables at the nodes are obtained by second-order interpolation.[43] Temporal integration is achieved by an explicit multistage modified Runge-Kutta method. Overall, the algorithm is second-order accurate in space and time. Full details of the algorithm are given in Knight.[28]

The boundary conditions are identical to the description of the structured grid code, except at the outer boundary where freestream conditions are imposed.

The unstructured grid of triangles were generated in two steps. First, the cell nodes were generated using the GRAPE program of Sorenson.[44] Second, the Delaunay triangulation was obtained from the UNSTRUCT program of Merriam.[45]

2. Validation of Algorithm

A series of test computations were performed to establish the accuracy of the unstructured grid algorithm.

a) Flat plate boundary layer. The freestream Mach number M_∞ was 2.0 and the Reynolds number Re_L was 3.95×10^4. The Prandtl number Pr was assumed to be 1 along with a linear viscosity law $\mu/\mu_\infty = T/T_\infty$. The grid employed 7802 triangular cells comprising 47 rows of 166 cells each. The number of grid points within the boundary layer was $N_{BL} = 23$ at $x = L$. The computed velocity and static temperature profiles agreed with the analytical profiles[32] within 2%.

b) Stationary airfoil (NACA-0012). The flow conditions were the same as the previous computation of a stationary NACA-0012 airfoil by the structured grid. The grid employed 25,534 cells. The average normal distance of the nodes adjacent to the airfoil surface was $\Delta n = 2.0 \times 10^{-3}c$. Measured in a direction normal to the airfoil surface, there were typically 14 nodes contained within the height of the boundary layer at the midchord. The grid spacing tangential to the airfoil surface varied from $\Delta s = 4.7 \times 10^{-3}c$ to $2.7 \times 10^{-2}c$, with the finest grid employed near the leading and trailing edges.

The drag coefficient computed from the unstructured grid calculation showed close agreement with the computations employing the structured grid and the previous computations of Beran[40] and Mehta[12] (Table 1). Detailed comparison of the computed flowfields showed close agreement with the structured grid calculations.[28]

D. Definition of Problem

The focus of the research is the understanding of the incipient leading-edge separation for subsonic viscous flow past an NACA-0012 airfoil pitching about the quarter chord axis

at $Re_c = 10^4$, $M_\infty = 0.2$ and $\Omega_0^+ = 0.2$. The flow configuration is shown in Fig. 2. The pitching motion, defined by Eq. (1), was initiated after the flowfield had been fully established at $\alpha = 0$ deg. The initial flowfield displayed a slight unsteadiness due to the periodic vortex shedding at the trailing edge. In particular, the amplitude of the lift coefficient c_l was 0.0146, and the dimensionless frequency was $fc/U_\infty = 2.05$. All computations were initiated at the peak in the lift coefficient; however, the results presented herein are insensitive to the relative phase of the initiation of the pitching motion.

An extensive grid refinement study was performed for the structured grid algorithm and indicated achievement of highly accurate solutions. Four separate grids were employed (Table 2). Case 2 represents a twofold refinement of the grid in the ξ and η directions relative to case 1. Cases 3 and 4 represent an approximate twofold refinement of the grid in either the ξ or η direction relative to case 2. (Limitations in computer memory precluded further simultaneous refinement in both the ξ and η directions.) A nondimensional time step ($dt^+ = tU_\infty/c$) of 1.0×10^{-3} was employed for all of the four cases. A study of the effect of the time step on the computed results showed the insensitivity of the selected time step on the computed results.[46] A comparison of lift c_l, drag c_d, and moment $c_{m_{ac}}$ coefficients for all four cases shows close agreement (Fig. 3). In particular, the lift and drag coefficients for cases 3 and 4 agree to within 1.5% for $0 < \alpha < 22.5$ deg, and the moment coefficients to within 3%. The computed streamlines for cases 3 and 4 are indistinguishable for $0 < \alpha < 21$ deg.

Table 2 NACA-0012 airfoil ($Re_c = 10^4$, $M_\infty = 0.2$, $\Omega\hat{t} = 0.2$)

Structured Grid					
Case	N_ξ	N_η	$\Delta n/c \times 10^4$	$\Delta s/c \times 10^3$	N_{BL}
1	319	91	2.0	3.38	32
2	637	181	1.0	1.69	64
3	1011	181	1.0	0.84	64
4	637	325	0.5	1.69	112
Unstructured Grid					
Case	*i*cell	*j*node	$\Delta n/c \times 10^4$	$\Delta s/c \times 10^3$	N_{BL}
5	30,238	15,299	10.0	3.5	14

N_ξ = Number of points in ξ direction.
N_η = Number of points in η direction.
Δn = Average normal distance of points next to airfoil.
Δs = Minimum tangential distance of points on airfoil.
N_{BL} = Number of points in boundary layer measured normal to airfoil surface at midchord for $\alpha = 0$ deg.
*i*cell = Number of triangles.
*j*node = Number of nodes.

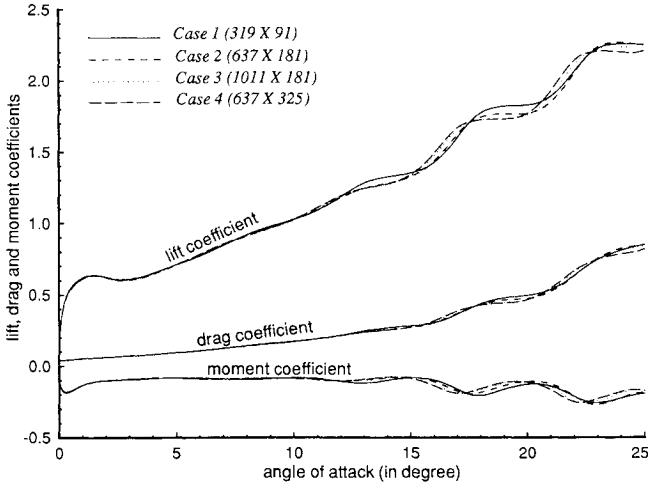

Fig. 3 Lift, drag, and moment coefficients for NACA-0012 airfoil using structured grid algorithm.

One computation was performed using the unstructured grid algorithm for comparison with the structured grid solutions. Details of the grid are presented in Table 2. Based on a temporal refinement study, a nondimensional time step ($dt^+ = tU_\infty/c$) of 2.6×10^{-5} was selected for this case.

III. Critical Point Theory

The understanding of unsteady separation for a pitching airfoil is greatly facilitated by visualization of the instantaneous streamlines (of course, the instantaneous streamlines are not identical to the particle pathlines or streaklines since the flow is unsteady). There are several possible frames of reference including 1) the inertial (laboratory) frame of reference wherein the freestream velocity is fixed and the velocity at the airfoil surface is generally nonzero, and 2) the rotating frame of reference (attached to the airfoil) wherein the freestream velocity is unsteady and the velocity at the airfoil surface is zero. The rotating frame possesses the seemingly intuitive advantage for physical interpretation of "forward" and "reverse" flow relative to the airfoil. Since the velocity is zero at the airfoil surface in the rotating frame of reference, the fluid immediately adjacent to a point on the airfoil surface is either instantaneously moving forward (i.e., toward the trailing edge) or reverse (i.e., toward the leading edge).

The instantaneous streamlines in the rotating frame of reference were selected for analysis. The components of the velocity (u', v') in the rotating frame of reference (x', y') are related to the components of the velocity (u, v) in the inertial frame by (Fig. 2)

$$\begin{aligned} u' &= +\Omega y' + u\cos\theta + v\sin\theta \\ v' &= -\Omega x' - u\sin\theta + v\cos\theta \end{aligned} \tag{2}$$

Note that the pitch rate $\Omega < 0$ for clockwise (pitch up) rotation. The instantaneous streamlines are

$$\begin{aligned} \frac{dx'}{d\tau} &= u'(x', y', t) \\ \frac{dy'}{d\tau} &= v'(x', y', t) \end{aligned} \tag{3}$$

where τ is the parametric length (with units of time) along the instantaneous streamlines at a particular time t.

Equation 3 is an autonomous system of ordinary differential equations which may possess critical points, i.e., loci where $u' = v' = 0$. The behavior of the equations in the vicinity of these critical points is well known as described, for example, in Kaplan[47] and Pontryagin.[48] Recent papers by Perry and Chong[49] and Chong et al.[50] have elucidated further details regarding fluid motions near critical points. The critical points may be classified on the basis of the Jacobian J and dilatation Δ where

$$J = \frac{\partial u'}{\partial x'}\frac{\partial v'}{\partial y'} - \frac{\partial u'}{\partial y'}\frac{\partial v'}{\partial x'} \tag{4}$$

$$\Delta = \frac{\partial u'}{\partial x'} + \frac{\partial v'}{\partial y'} \tag{5}$$

The taxonomy of critical points for two-dimensional flow is described in Fig. 4. For $J < 0$, the topology is a saddle, with the relative orientation of the asymptotes determined by the value of Δ. For $J > 0$ the principal topologies are nodes and foci, with the latter obtained for $J > \Delta^2/4$. The patterns are stable (i.e., the instantaneous fluid motion is toward the critical point) or unstable (i.e., the instantaneous fluid motion is away from the critical point) based on the sign of Δ. In those instances where $\Delta = 0$, the topology changes from a saddle

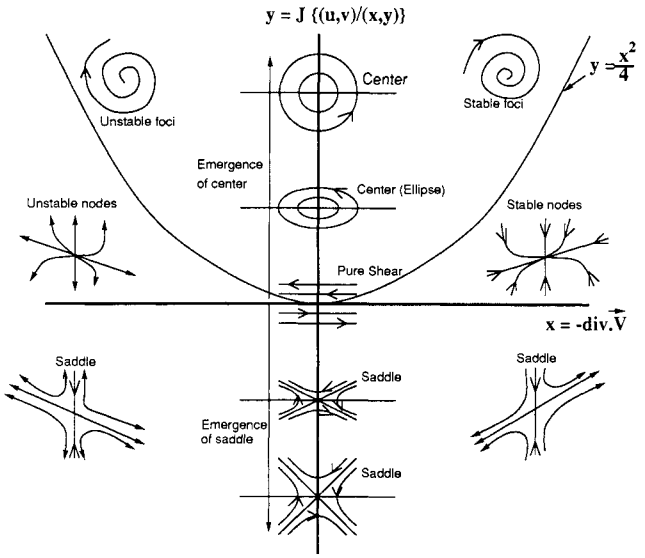

Fig. 4 Classification of critical points.

(for $J < 0$), to a simple shear (for $J = 0$) and center (for $J > 0$).

IV. Results

A. Structured Grid

The instantaneous streamlines and vorticity obtained from the structured grid computation (case 3) are displayed in the vicinity of the leading edge (arbitrarily defined as the first 30% of the chord) in Figs. 5–9 for $\alpha = 14.5$, 16.5, 19.5, 21.0, and 22.5 deg. All results are based on a reference frame attached to the airfoil. The airfoil-attached reference frame allows an unambiguous definition of forward (or "attached") and reversed flow within a thin unseparated boundary layer, since the velocity of the fluid at the airfoil surface is zero. Forward flow is defined as fluid moving toward the trailing edge, and reversed flow indicates fluid moving toward the leading edge. Also shown are two particles, colored red and black, which were released initially within the boundary layer at the leading edge at a height of $2.04 \times 10^{-4}c$ and $4.32 \times 10^{-4}c$ from the airfoil surface, respectively, at the start of the airfoil rotation.

At $\alpha = 14.5$ deg, the flow on the upper surface in the vicinity of the leading edge has a thin reversed flow region extending to 7% chord position, and there are no critical points in the vicinity of the leading edge [the flow near the trailing edge (not shown) displays a complex separation behavior] within the flow, though, there is a half-saddle point that appears on the airfoil surface near the leading edge and represents the farthest upstream extent of the reversed flow adjacent to the airfoil. The red boxed region in Fig. 5 has been enlarged in Figs. 10–12 at $\alpha = 14.75$, 14.99, and 15.01 deg. The enlarged figures show the stages in the formation of the primary recirculating region near the leading edge. At $\alpha = 14.75$ deg, reversed flow can be seen near the leading edge but there are no critical points within the flow in the vicinity of the leading edge. The instantaneous streamlines in the region between forward and reversed flow are in the shape of a C. As α increases, one of the C-shaped instantaneous streamlines collapses at a single point. At $\alpha = 14.99$ deg, the instantaneous streamlines show the first appearance of a pair of critical points in the flowfield near the leading edge at 18% chord position and a distance $2.5 \times 10^{-3}c$ above the airfoil surface. The critical point initially appears as a single point corresponding to a pure shear, i.e., $J = \Delta = 0$ (Fig. 4). It immediately bifurcates into two critical points (a center and a saddle) as shown in Fig. 11. At the instant shown in Fig. 11, the critical point has already bifurcated into a center and a saddle. The two critical points move apart and the center gives rise to the primary recirculating region with a clockwise sense of rotation (Fig. 12).

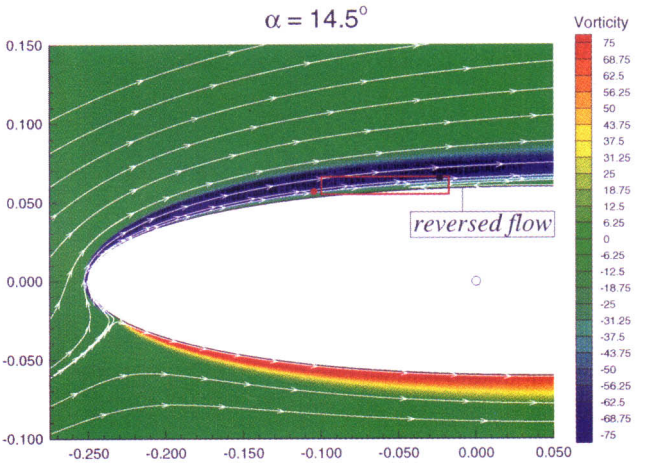

Fig. 5 Computed flowfield at $\alpha = 14.5$ deg using structured grid; instantaneous streamlines, vorticity contours, and location of two particles.

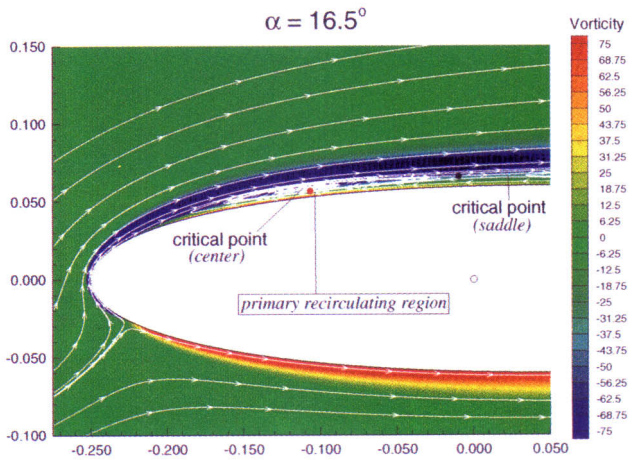

Fig. 6 Computed flowfield at $\alpha = 16.5$ deg using structured grid; instantaneous streamlines, vorticity contours, and location of two particles.

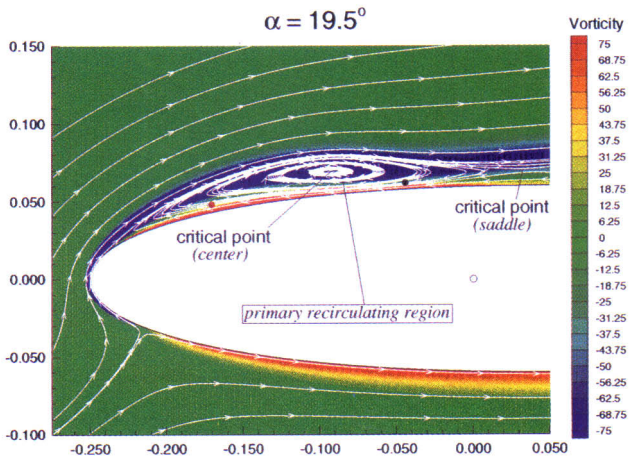

Fig. 7 Computed flowfield at $\alpha = 19.5$ deg using structured grid; instantaneous streamlines, vorticity contours, and location of two particles.

At $\alpha = 16.5$ deg (Fig. 6), the critical points have moved farther apart. The leftmost critical point (a center), and the rightmost critical point (a saddle), correspond to positive and negative values of the Jacobian, respectively (Fig. 4). The

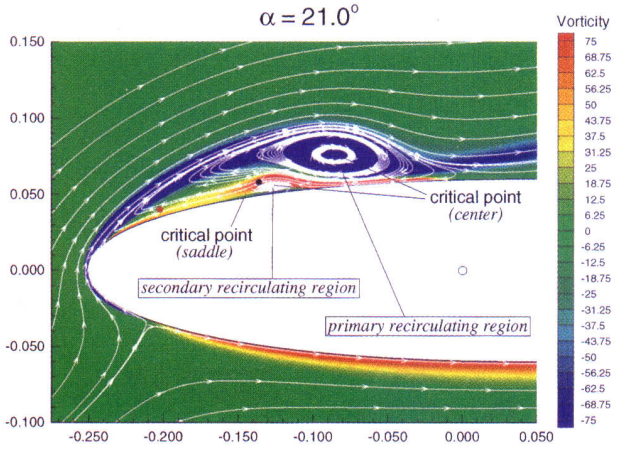

Fig. 8 Computed flowfield at α = 21.0 deg using structured grid; instantaneous streamlines, vorticity contours, and location of two particles.

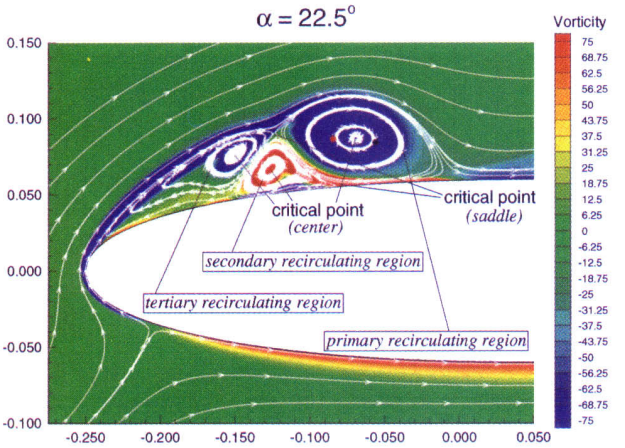

Fig. 9 Computed flowfield at α = 22.5 deg using structured grid; instantaneous streamlines, vorticity contours, and location of two particles.

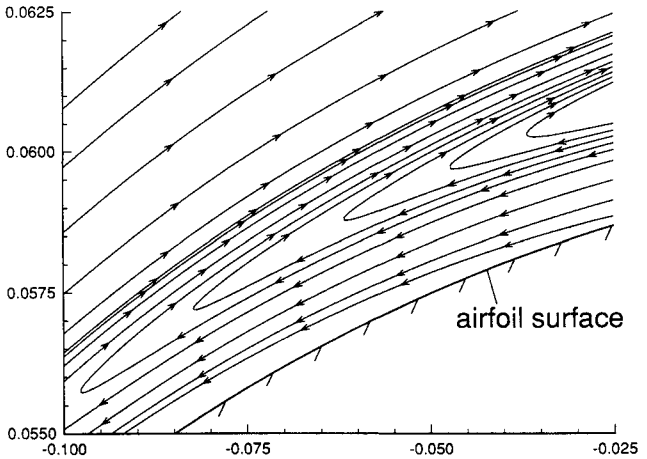

Fig. 10 Instantaneous streamlines at α = 14.75 deg; before the birth of primary recirculating region.

dilatation remains essentially zero. The center marks the primary recirculating region, which eventually leads to the boundary-layer separation and (ultimately) dynamic stall. At α = 19.5 deg (Fig. 7), the primary recirculating region has grown in transverse direction, which is reflected in the increased magnitude of the Jacobian. The saddle point has moved slightly downstream.

At α = 21.0 deg (Fig. 8), a second pair of critical points have appeared near the upper surface at approximately 10% chord (saddle point) and 13% chord (center). A secondary recirculating region forms about the second center with counterclockwise rotation. The primary recirculating region has grown farther in transverse dimension. The first saddle point has migrated to the airfoil surface at 28% chord and become a half-saddle. Another half-saddle point is present on the upper surface at 2% chord. The instantaneous streamline emanating from the upstream half-saddle point encompasses the two recirculating regions and approaches the downstream half-saddle point.

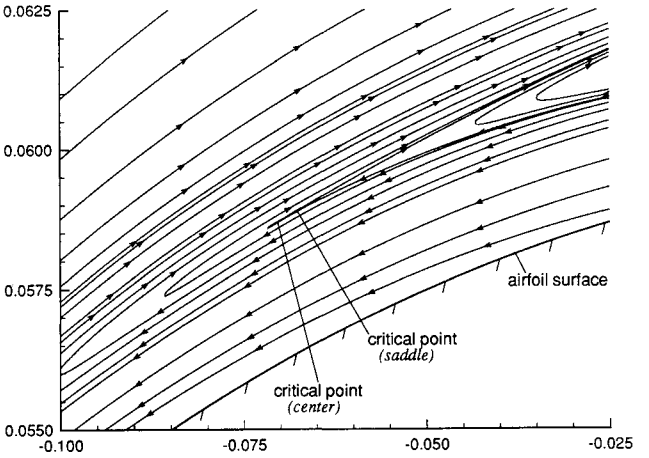

Fig. 11 Instantaneous streamlines at α = 14.99 deg; birth of primary recirculating region.

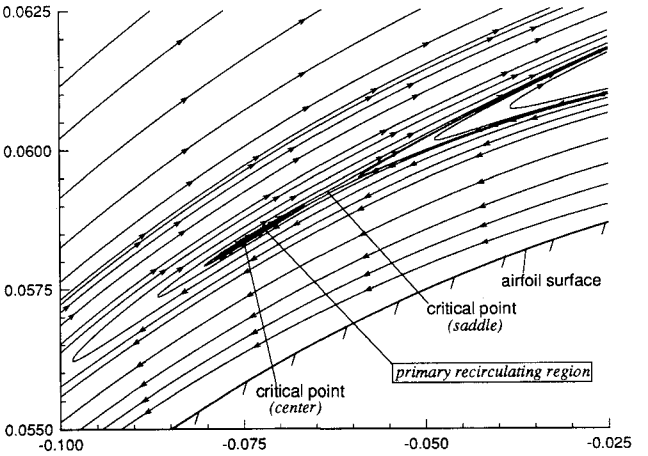

Fig. 12 Instantaneous streamlines at α = 15.01 deg; growth of primary recirculating region.

At α = 22.5 deg, a third pair of critical points have emerged to form a tertiary recirculating region and saddle point. The sense of rotation of the tertiary recirculating region is clockwise. At subsequently larger values of α, the primary recirculating region "detaches" from the boundary during the formation of the dynamic stall vortex.

The relationship between the birth of the critical points and the Moore-Rott-Sears (MRS) criterion has been studied. According to the MRS criterion, separation of the boundary layer corresponds to point of zero shear stress and zero velocity within the fluid in a frame of reference traveling with the separation region. If the airfoil attached coordinate axis is assumed to be the frame of reference considered by the MRS criterion, then the appearance of a critical point would signify separation in the MRS sense if the shear stress is zero at the critical point. The shear stress at all critical points is found to be nonzero and comparable to the shear stress at the wall, with the exception of the half-saddle points on the airfoil surface where the shear stress is necessarily zero. Therefore, the critical points within the flowfield are not separation points according to the MRS criterion.

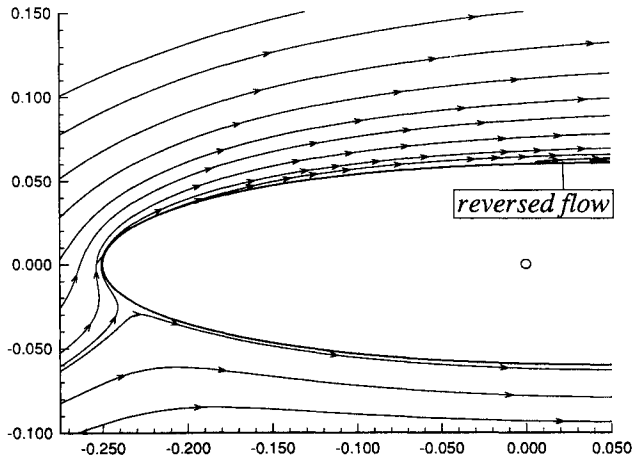

Fig. 13 Instantaneous streamlines at α = 14.5 deg for unstructured grid calculation.

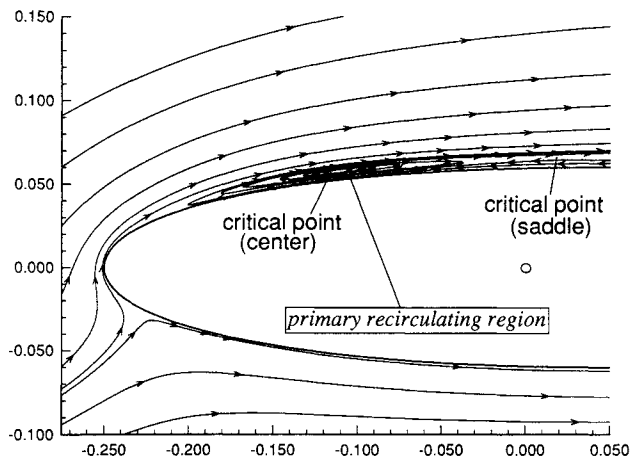

Fig. 14 Instantaneous streamlines at α = 16.5 deg for unstructured grid calculation.

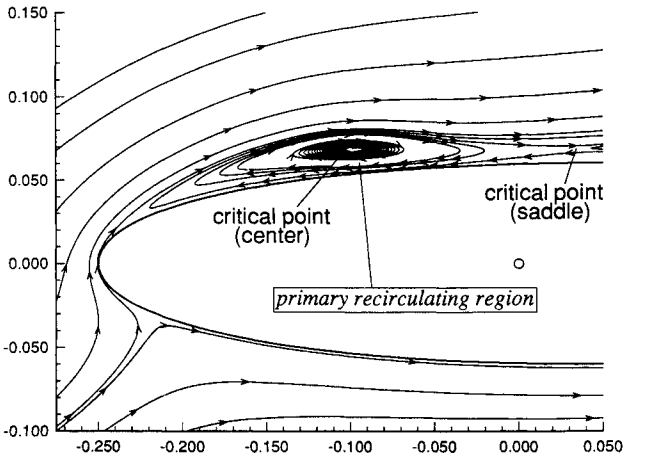

Fig. 15 Instantaneous streamlines at α = 19.5 deg for unstructured grid calculation.

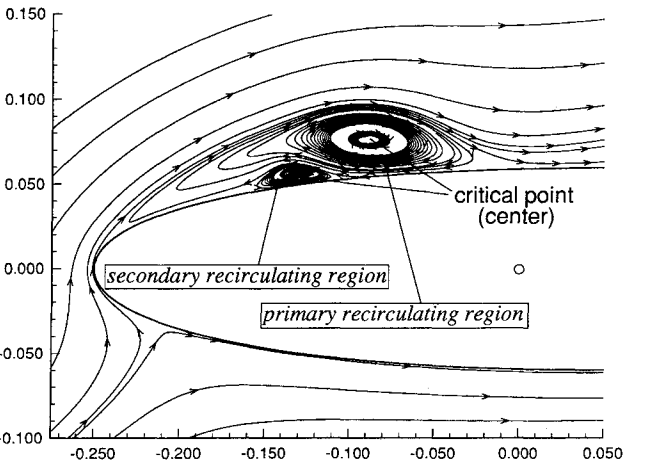

Fig. 16 Instantaneous streamlines at α = 21.0 deg for unstructured grid calculation.

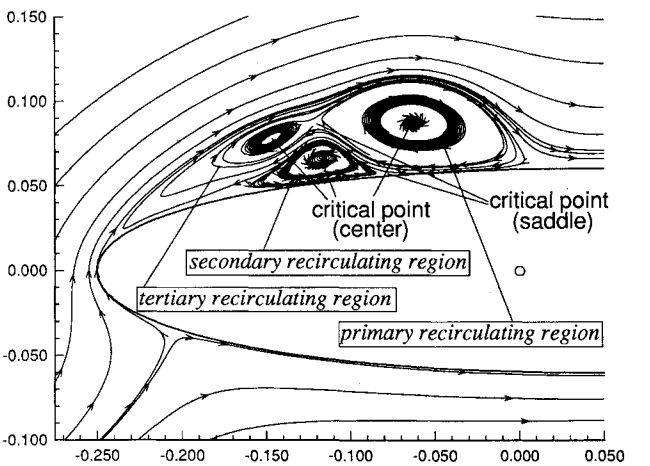

Fig. 17 Instantaneous streamlines at α = 22.5 deg for unstructured grid calculation.

The locations of two particles released in the flowfield are shown in Figs. 5–9. A number of other particles were also released in the flowfield and the conclusions presented here have been drawn after studying all such particles released. The instantaneous streamlines show the reversed flow region reaching the leading edge at about α = 15 deg, and the particle traces confirm it. Figure 6 shows the red particle moving toward the leading edge whereas the black particle, which was released at a distance above the red particle from the leading edge, moving toward the trailing edge. This shows that the reversed flow is contained in a very thin region near the surface. Figure 7 shows both particles moving toward the leading edge, indicating a thickening of the reversed flow region with increasing α. The reversed flow thickness increases with increasing α and expands rapidly for $\alpha > 18$ deg along with the expansion of the primary recirculating region. The particles released near the leading edge move away from the wall and then approach the surface at about the quarter chord position. The streamline plots in Figs. 8 and 9 display similar qualitative behavior. Figure 8 shows the two particles being caught in the primary recirculating region. Just after the secondary recirculating region forms over the airfoil, a three-layer structure appears near the wall. The bottom layer near the wall has forward flow. The intermediate layer has reversed flow, whereas the top layer has forward flow. The formation of the secondary recirculating region precedes the sudden ejection of the particles in a direction approximately normal to the airfoil surface, which indicates the boundary-layer separation. The two particles which were released very near the airfoil surface are seen at a distance from the airfoil surface which is comparable to the boundary-layer thickness (Fig. 9). The ejection of the particles is aided by the three-layer structure, which gives rise to forward and reversed flow on the two sides of the point of ejection. The mechanism of

eruption of the boundary layer is found to be similar to the one discussed by Peridier et al.[21,22] The secondary and the primary recirculating regions interact with each other and eject the fluid from the airfoil surface.

The sequence of events just described may vary significantly at different flow conditions (Re_c, M_∞, Ω_0^+, and the nature of the pitching motion). Future research efforts will be focused on understanding the effects of these parameters on the initial stages of boundary-layer separation.

B. Unstructured Grid

Instantaneous streamlines obtained using the unstructured grid code are shown in Figs. 13–17 at α = 14.5, 16.5, 19.5, 21.0, and 22.5 deg. Overall, there is close agreement between the structured and unstructured grid computations. The primary recirculating region is evident in both cases at α = 16.5 deg, and has grown at α = 19.5 deg. The secondary and tertiary recirculating regions at α = 22.5 deg are quantitatively very similar in both computations. The close comparison between the separate computations using two fundamentally different algorithms lends substantial credibility to the results.

V. Conclusions

The initial stages of boundary-layer separation on a NACA-0012 airfoil pitching about its quarter chord axis at $Re_c = 10^4$, $M_\infty = 0.2$, and $\Omega_0^+ = 0.2$ have been studied using two separate numerical algorithms based on a structured and unstructured grid, respectively. The principal results are as follows.

1) The emergence of the primary recirculating region has been traced to a pair of critical points (a center and a saddle) that first appear within the flowfield at α = 14.99 deg at the 18% chord location and a distance $2.5 \times 10^{-3}c$ above the airfoil. The primary recirculating region (center) has a clockwise sense of fluid rotation and grows with increasing α.

2) The critical points in the flowfield in a reference frame attached to the airfoil do not signify boundary-layer separation in the sense of Moore-Rott-Sears.

3) Secondary and tertiary recirculating regions form after the appearance of the primary recirculating region. The sense of fluid rotation is counter clockwise and clockwise, respectively. The secondary recirculating region interacts with the primary recirculating region to eject the fluid close to the wall in a direction approximately normal to the wall. The ejection of the fluid near the wall signifies boundary-layer separation.

4) The accuracy of the computations has been confirmed by the close agreement between the structured and unstructured grid computations and the grid refinement study for the structured grid computations.

Acknowledgments

This research was sponsored by the Army Research Office under Grant DAAL03-91-G-0096, monitored by Tom Doligalski. Supercomputer resources have been provided by the NASA-Ames Research Center. The results have been analyzed at the Rutgers University-Supercomputer Remote Access Center.

References

[1]Stepniewski, W., and Keys, C., *Rotary-Wing Aerodynamics*, Dover, New York, 1984, pp. 1–42.

[2]Rott, N., "Unsteady Viscous Flow in the Vicinity of a Stagnation Point," *Quarterly of Applied Mathematics*, Vol. 13, No. 4, 1956, pp. 444–451.

[3]Sears, W. R., and Telionis, D. P., "Boundary Layer Separation in Unsteady Flow," *SIAM Journal of Applied Mathematics*, Vol. 28, No. 1, 1975, pp. 215–235.

[4]Carr, L., "Progress in Analysis and Prediction of Dynamic Stall," *Journal of Aircraft*, Vol. 25, Jan. 1988, pp. 6–17.

[5]Carr, L. W., and McCroskey, W. J., "A Review of Recent Advances in Computational and Experimental Analysis of Dynamic Stall," International Union of Theoretical and Applied Mechanics Symposium on Fluid Dynamics of High Angle of Attack, Tokyo, Japan, Sept. 1992.

[6]McCroskey, W. J., Carr, L., and McAlister, K., "Dynamic Stall Experiments on Oscillating Airfoils," *AIAA Journal*, Vol. 14, No. 1, 1976, pp. 57–63.

[7]Acharya, M., and Metwally, M., "Evolution of the Unsteady Pressure Field and Vorticity Production at the Surface of a Pitching Airfoil," AIAA Paper 90-1472, 1990.

[8]Chandrashekhara, M., and Ahmed, S., "Laser Velocimetry Measurements of Oscillating Airfoil Dynamic Stall Flow Field," AIAA Paper 91-1799, 1991.

[9]Carr, L., Chandrashekhara, M., and Brock, N., "A Quantitative Study of Unsteady Compressible Flow on an Oscillating Airfoil," AIAA Paper 91-1683, 1991.

[10]Chandrashekhara, M., and Carr, L., "Flow Visualization of the Mach Number Effects on the Dynamic Stall of an Oscillating Airfoil," AIAA Paper 89-0023, 1989.

[11]Mehta, U. B., and Zalman, L., "Starting Vortex, Separation Bubbles and Stall: A Numerical Study of Laminar Unsteady Flow Around an Airfoil," *Journal of Fluid Mechanics*, Vol. 67, Pt. 2, 1975, pp. 227–256.

[12]Mehta, U. B., "Dynamic Stall of an Oscillating Airfoil," *Unsteady Aerodynamics*, AGARD CP-227, 1977, pp. 23.1–23.32.

[13]Ghia, K. N., Yang, J., Osswald, G. A., and Ghia, U., "Study of the Dynamic Stall Mechanism Using Simulation of Two-Dimensional Navier-Stokes Equations," AIAA Paper 91-0546, 1991.

[14]Ghia, K. N., Yang, J., Osswald, G. A., and Ghia, U., "Study of the Role of Unsteady Separation in the Formation of Dynamic Stall Vortex," AIAA Paper 92-0196, 1992.

[15]Walker, J. M., Helin, H. E., and Strickland, J. H., "An Experimental Investigation of an Airfoil Undergoing Large Amplitude Pitching Motions," *AIAA Journal*, Vol. 23, No. 8, 1985, pp. 1141, 1142.

[16]Visbal, M. R., "On the Formation and Control of the Dynamic Stall Vortex on a Pitching Airfoil," AIAA Paper 91-0006, 1991.

[17]Visbal, M. R., "Dynamic Staff of a Constant-Rate Pitching Airfoil," *Journal of Aircraft*, Vol. 27, No. 5, 1990, pp. 400–407.

[18]Smith, F. T., "Concerning Dynamic Stall," *The Aeronautical Quarterly*, Vol. 33, Nov. 1982, pp. 331–352.

[19]Smith, F. T., F. R. S., and Elliott, J. W., "On the Abrupt Turbulent Reattachment Downstream of Leading-edge Laminar Separation," *Proceedings of The Royal Society of London A*, Vol. 401, Sept. 1985, pp. 1–27.

[20]Smith, F. T., "Finite-time Break-up can Occur in Any Unsteady Interacting Boundary Layer," *Mathematika*, Vol. 35, No. 70, 1988, pp. 256–273.

[21]Peridier, V. J., Smith, F. T., and Walker, J. D. A., "Vortex-induced Boundary-layer Separation. Pt. 1, The Limit Problem Re $\rightarrow \infty$," *Journal of Fluid Mechanics*, Vol. 232, Nov. 1991, pp. 99–131.

[22]Peridier, V. J., Smith, F. T., and Walker, J. D. A., "Vortex-induced Boundary-layer Separation. Pt. 2, Unsteady Interacting Boundary-layer Theory," *Journal of Fluid Mechanics*, Vol. 232, Nov. 1991, pp. 133–165.

[23]Van Dommelen, L. L., and Cowley, S. J., "On the Lagrangian Description of Unsteady Boundary-layer Separation. Pt. 1, General Theory," *Journal of Fluid Mechanics*, Vol. 210, Jan. 1990, pp. 593–626.

[24]Smith, F. T., "Steady and Unsteady Boundary Layer Separation," *Annual Review of Fluid Mechanics*, Vol. 18, 1986, pp. 197–220.

[25]Walker, J., "Unsteady Boundary Layer Separation in Two-Dimensional Flows," Workshop on Supermaneuverability: Physics of Unsteady Separated Flows at High Angle of Attack, Lehigh Univ., Bethlehem, PA, 1992.

[26]Walker, J., "Issues Relating to Unsteady Separation at High Reynolds Number," 1992 Computational Fluid Dynamics Symposium, Wright-Patterson AFB, OH, Sept. 1992.

[27]Beam, R. M., and Warming, R. F., "An Implicit Factored Scheme for the Compressible Navier-Stokes Equations," *AIAA Journal*, Vol. 15, No. 4, 1978, pp. 393–402.

[28]Knight, D., "A Fully Implicit Navier-Stokes Algorithm Using an Unstructured Grid and Flux-Difference Splitting," AIAA Paper 93-0875, 1993.

[29]Roe, P., "Approximate Riemann Solvers, Parameter Vectors, and Difference Schemes," *Journal of Computational Physics*, Vol. 43, No. 2, 1981, pp. 357–372.

[30]McCroskey, W. J., and Philippe, J., "Unsteady Viscous Flow on Oscillating Airfoils," *AIAA Journal*, Vol. 13, No. 1, 1975, pp. 71–79.

[31]Steger, J., "Implicit Finite-Difference Simulation of Flow About Arbitrary Two-Dimensional Geometries," *AIAA Journal*, Vol. 16, No. 7, 1978, pp. 679–686.

[32]White, F. M., *Viscous Fluid Flow,* McGraw-Hill, New York, 1974, pp. 28–30, 261–267.

[33]Pulliam, T. H., "Artificial Dissipation Models for the Euler Equations," *AIAA Journal*, Vol. 24, No. 12, 1986, pp. 1931–1940.

[34]Visbal, M. R., and Shang, J. S., "Investigation of the Flow Structure Around a Rapidly Pitching Airfoil," *AIAA Journal*, Vol. 27, No. 8, 1989, pp. 1044–1051.

[35]Thomas, J. L., and Salas, M. D., "Far-Field Boundary Conditions for Transonic Lifting Solutions to the Euler Equations," *AIAA Journal*, Vol. 24, No. 7, 1986, pp. 1074–1080.

[36]Visbal, M. R., "Calculations of Viscous Transonic Flows About a Supercritical Airfoil," Air Force Wright Aeronautical Lab., AFWAL-TR-86-3013, July 1986.

[37]Visbal, M. R., "Evaluation of an Implicit Navier-Stokes Solver for Some Unsteady Separated Flows," AIAA Paper 86-1053, 1986.

[38]Thomas, P. D., and Lombard, C. K., "Geometric Conservation Law and its Applications to Flow Computations on Moving Grids," *AIAA Journal*, Vol. 17, No. 10, 1979, pp. 1030–1037.

[39]Kinsey, D. W., and Barth, T. J., "Description of a Hyperbolic Grid Generating Procedure for Arbitrary Two-Dimensional Bodies," Air Force Wright Aeronautical Lab., AFWAL-TM-84-191-FIMM, July 1984.

[40]Beran, P., "Steady and Unsteady Solutions of the Navier-Stokes Equations for Flows About Airfoils at Low Speeds," AIAA Paper 91-1733, 1991.

[41]Whittaker, D., Slack, R., and Walters, R., "Solution Algorithm for the Two-Dimensional Euler Equations on Unstructured Meshes," AIAA Paper 90-0697, 1990.

[42]Martinelli, L., and Jameson, A., "Validation of a Multigrid Method for the Reynolds Averaged Equations," AIAA Paper 88-0414, 1988.

[43]Rausch, R., Batina, J., and Yang, H., "Spatial Adaption Procedures on Unstructured Meshes for Accurate Unsteady Aerodynamic Flow Computation," AIAA Paper 91-1106, 1991.

[44]Sorenson, R. L., "A Computer Program to Generate Two-Dimensional Grids About Airfoils and Other Shapes by the Use of Poisson's Equation," Ames Research Center, NASA TM 81198, Moffett field, CA, May 1980.

[45]Merriam, M., "UNSTRUCT—An Unstructured Grid Generator for the Iris Workstation," NASA Ames Research Center, 1991.

[46]Choudhuri, P. G., Knight, D. D., and Visbal, M. R., "2-D Unsteady Separation on a Pitching Airfoil," *1993 ASME Division of Fluid Engineering Summer Meeting—Forum on Unsteady Flows,* FED-Vol. 157, June 1993, pp. 1–12.

[47]Kaplan, W., *Ordinary Differential Equations*, Addison-Wesley, Reading, MA, 1958, p. 415–423.

[48]Pontryagin, L. S., *Ordinary Differential Equations*, Addison-Wesley, Reading, MA, 1962, pp. 103–126.

[49]Perry, A. E., and Chong, M. S., "A Description of Eddying Motions and Flow Patterns Using Critical-Point Concepts," *Annual Review of Fluid Mechanics*, Vol. 19, 1987, pp. 125–155.

[50]Chong, M., Perry, A., and Cantwell, B., "A General Classification of Three-Dimensional Flow Fields," *Topological Fluid Dynamics*, Proceedings of the International Union of Theoretical and Applied Mechanics Symposium, edited by H. Moffatt and A. Tsinober, Cambridge Univ. Press, 1990.